American Mineralogist, Volume 92, pages 954–965, 2007

Chemical composition, statistical analysis of the unit cell, and electrostatic modeling of the structure of Al-saturated chlorite from metamorphosed rocks

Sang Soo Lee,[1] Stephen Guggenheim,[1,*] M. Darby Dyar,[2] and Charles V. Guidotti[3,†]

[1]Department of Earth and Environmental Sciences, University of Illinois at Chicago, Chicago, Illinois 60607, U.S.A.
[2]Department of Earth and Environment, Mount Holyoke College, South Hadley, Massachusetts 01075, U.S.A.
[3]Department of Geological Sciences, University of Maine, Orono, Maine 04401-5711, U.S.A.

Abstract

Natural Al-saturated chlorite having a wide range of Mg:Fe ratios [Mg/(Mg + Fe) = 0.357 to 0.943] was studied to determine the effect of Mg-Fe substitution on the unit-cell parameters. With a nearly constant Al content [$Al_T/(Al_T + Mg + Fe)$ = 0.362 to 0.416, where Al_T represents total Al contents in both tetrahedral and octahedral sites], the only major variable affecting the unit-cell dimensions of natural chlorite is the Mg:Fe ratio. The value of about 0.4 for the Al content represents apparent Al saturation for chlorites in metamorphosed rocks. Unit-cell parameters were determined by least-squares refinement from 39 chlorite samples obtained over a large range in metamorphic grades, from X-ray data derived from Gandolfi pattern simulations (via single crystals and a single-crystal diffractometer) from this study and from traditional powder diffractometer data from the literature. Nine of the samples were analyzed for their Fe^{3+} contents (= 0.147 to 0.304 atoms) by Mössbauer spectroscopy; chemical compositions were generally obtained by electron-microprobe analysis.

Statistical tests show that the change of the crystallographic *a* and *b* axes are linear over the range of Mg:Fe ratios studied, whereas the crystallographic *c* axis and the β angle have no significant relationship to these Mg:Fe ratios. Equations relating the effect of Mg:Fe ratio on *a* and *b* are: *a* (Å) = −0.092 *x* + 5.408; *x* = Mg/(Mg + Fe) and *b* (Å) = − 0.162 *x* + 9.370, respectively.

Electrostatic models involving Pauling's electrostatic valency principle for Al-saturated chlorite were determined assuming: (1) Al-Al avoidance for Al-substituted tetrahedra, (2) no vacancies, and (3) no Al^{3+} substitution in the M1 sites. Electrostatic restrictions occur for $R^{3+} \rightarrow R^{2+}$ substitutions in the M2 sites of the 2:1 layer. These restrictions produce an Al saturation in chlorite at $Al_T/(Al_T + Mg + Fe)$ ratios of near 0.4. This saturation limit requires that 37.5% of the tetrahedral sites (1.5 out of 4 sites) are occupied by Al, and the electrostatic charge (electrostatic valency units, e.v.u.) close to +1 e.v.u. is favored for the interlayer to offset the net negative charge on the 2:1 layer.

Keywords: Al-saturated chlorite, Gandolfi powder-pattern simulations, Mössbauer spectroscopy, Mg,Fe effects on chlorite unit cell, electrostatic modeling, layer charge

Introduction

Chlorite, $^{VI}(R^{2+}_{6-x-3y}\ Al_{x+2y}\ \square_y)^{IV}(Si_{4-x}\ Al_x)O_{10}\ (OH)_8$ where R^{2+} = (Mg + Fe^{2+}) and □ = vacancy, is a common phyllosilicate constituent of calc-silicate, pelitic, mafic, and ultramafic rocks, and it is stable over a range of low- to medium-grade metamorphic conditions. Chlorite incorporates medium-size octahedral cations, primarily Mg, Fe^{2+}, Fe^{3+}, Al^{3+}, and occasionally Cr, Mn, Ni, V, Cu, Zn, and Li. Various studies have suggested that the unit-cell parameters of chlorite vary linearly with chemical composition (Shirozu 1958; Bailey 1972; Jenkins and Chernosky 1986; Roots 1994; Baker and Holland 1996). However, because of the many possible chemical constituents that may enter the structure and the many possible sites for chemical substitutions (four unique octahedral sites and two unique tetrahedral sites for the II*b* polytype, common to higher-temperature assemblages), determining the effect of substituting elements on unit-cell dimensions may be problematic (e.g., see Eggleton and Bailey 1967; Shirozu and Higashi 1976; Bailey 1988). Using synthetic chlorite is one way to minimize the chemical variations because the composition of the chlorite can be controlled by changing the bulk chemistry and by maintaining careful control of the experiments to ensure the appropriate oxygen fugacity. However, Jenkins and Chernosky (1986) showed that the length of the *c* axis of synthetic Mg- and Al-rich chlorite is sensitive to the presence of co-existing phases, presumably because of elemental (Mg, Al) partitioning between coexisting phases. Therefore, it is difficult to obtain consistent unit-cell parameters for chlorite at a given bulk composition from synthesis work.

The interlayer M4 site in the chlorite structure exhibits large thermal expansion (Nelson and Guggenheim 1993) but contains the smaller trivalent cations (Phillips et al. 1980). Nelson and Guggenheim suggested that the interlayer M3 site does not accept trivalent cations readily because of the high charge of these cations and M3-M3 and M3-M4 repulsions. Furthermore, any Fe^{2+} iron in M4 cannot easily oxidize to Fe^{3+} at elevated

* E-mail: xtal@uic.edu
† Deceased, May 19, 2005.

0003-004X/07/0506–954$05.00/DOI: 10.2138/am.2007.2309

temperatures because of the large thermal expansion of M4 and the instability of having a small trivalent cation in a large site (e.g., Goldschmidt's rule). Nelson and Guggenheim also noted that the ordering of trivalent cations in the interlayer M3 site is destabilizing because of electrostatic repulsions that would affect the hydrogen bond network, the in-plane rotation of Si, Al tetrahedra, and the lateral expansion of the of the 2:1 layer. Thus, the oxidation of Fe in chlorite appears to be limited and independent of temperature, as has been previously noted by Dyar et al. (1992) in a Mössbauer study.

To a good approximation, the compositional variation observed in the vast majority of metamorphic chlorites involves only four constituents: MgO, FeO, Al_2O_3, and SiO_2. For example, Laird (1988) showed a plot of chemical composition of chlorite from diverse geologic settings and found that the compositional variations are relatively restrictive to these constituents, although Mn, Ti, Fe^{3+}, and Cr generally occur as minor constituents, and that substitutions for OH are rare. Of particular interest is the well-defined upper limit to the Al content of chlorites. Most of the chlorites reported by Laird (1988, Fig. 2) had an atomic molar ratio of $Al_T/(Al_T + Mg + Fe)$ less than 0.4, where Al_T represents total Al content in chlorite, regardless of both rock type and Mg:Fe ratio. Because Si shows little variation when chlorite is saturated with Al, the only major variable in Al-saturated chlorite is the Mg:Fe ratio. One purpose of this study was to investigate the effect of Mg:Fe ratio on the chlorite structure, specifically unit-cell parameters, using natural samples of Al-saturated chlorite to minimize other variations in chlorite chemistry, including Si and Al contents. In addition, we present electrostatic models to explain why an upper Al limit exists for metamorphic chlorite.

Materials and methods

Sample selection and preparation

Twenty-three natural chlorite samples from Al-saturated metamorphic assemblages (Table 1) were analyzed in this study: (1) twenty samples were from the Siluro-Devonian metapelites in the southwest portion of the Rangeley Quadrangle of western Maine (Guidotti 1974; Guidotti et al. 1991); (2) one sample (CG/BG-1) was from the garnet-zone chlorite pseudomorphs after cordierite in the sulfide- and graphite-rich Smalls Falls Fm. at Black Mountain, Maine (to the south of the Rangeley localities) (Rumble 1971, 1978; Rumble et al. 1993); (3) one sample (CG/BG-6) was from chlorite pseudomorphs after staurolite in metapelites from the Perry Moutain in the Rangeley Quadrangle (see citations above); and (4) one sample (Likhanov 24) was from Altay-Sayan Fold Region, in West Siberia (Likhanov 1988a, 1988b).

From each sample, a thin section was made to allow for petrographic description and electron-microprobe analysis. From the remaining rock, areas with high concentrations of chlorites (usually in sprays) were carefully removed by cutting and gentle crushing. Single chlorite grains for X-ray diffraction (XRD) analysis were carefully selected from these areas. Further crushing and hand-picking under a binocular microscope were employed to obtain the 10–30 mg of sample needed for Mössbauer analysis of selected chlorite.

Chlorite in these rocks is often finely intergrown with biotite or sulfides, and could not be cleanly separated in all cases. Thus, in some cases it was not possible to obtain sufficiently pure chlorite for Mössbauer spectroscopy. For this reason, the samples for which we were able to obtain Mössbauer spectra do not fully match those on which we were able to obtain single-crystal (Gandolfi simulation) unit-cell refinements.

Chemical analysis

Chemical analyses were performed at the University of Maine for all samples studied using standard electron-microprobe techniques (Guidotti 1974) with a wavelength dispersive system (Table 2). Special care was taken to analyze all of the textural varieties of chlorite present in each polished thin section. In general, no differences in chemical composition were observed among the chlorite varieties, which implied that chlorite reached a chemical equilibrium in a given specimen (Guidotti et al. 1991). One pseudomorphic chlorite (CG/BG-6) showed a significantly high content of Fe^{3+} compared to the other samples (Tables 2 and 3) and was excluded from the regression analyses. In addition, 16 natural chlorite samples reported in the literature were included in the data set and used for statistical analyses. Chemical compositions of the chlorites nearly cover the entire range of Mg and Fe composition (Fig. 1, Table 2). Samples have values of $Al_T/(Al_T + Mg + Fe)$ in the range from 0.362 to 0.416, and these depart ≤10% from the value of 0.4 that presumably represents Al-saturated chlorite (Laird 1988, Fig. 2).

Mössbauer spectroscopy

Approximately 10–30 mg of sample were crushed to a fine powder with sugar under acetone before mounting in a sample holder confined by cellophane tape. The resultant sample thicknesses were approximately 1–3 mg Fe/cm^2, using the thin absorber calculation of Long et al. (1983). Mössbauer spectra were acquired at 293 K using a source of 100–30 mCi ^{57}Co in Rh on a WEB Research Co. model W100 spectrometer. Run times ranged from 24–96 hours, with non-resonant counts of 5–24 million, and results were calibrated against α-Fe foil.

Mössbauer spectra were fit with various different models. Room-temperature spectra of a limited number of samples were initially processed using the WMOSS software of WEB Research Co., which allows use of pure Lorentzian lineshapes, Voigt lineshapes, or quadrupole-splitting distributions (Rancourt and Ping 1991). Linewidth, Δ_0, δ_Δ, δ_0, and δ_1 were allowed to vary in many different combinations,

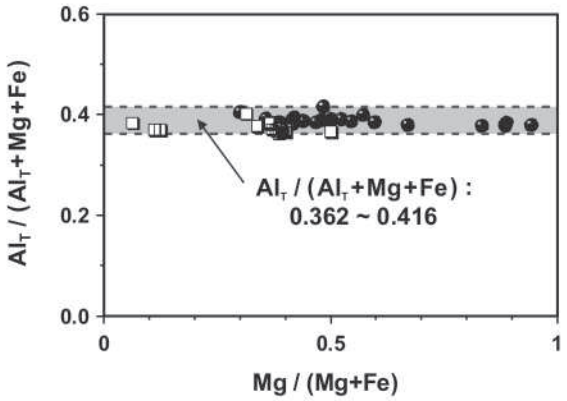

Figure 1. Atomic fraction $Al_T/(Al_T + Mg + Fe)$ vs. Mg/(Mg + Fe) of the chlorite data from this study (solid circles) and from the literature (open squares). The assemblages and compositions of the chlorites are given in Tables 1 and 2, respectively.

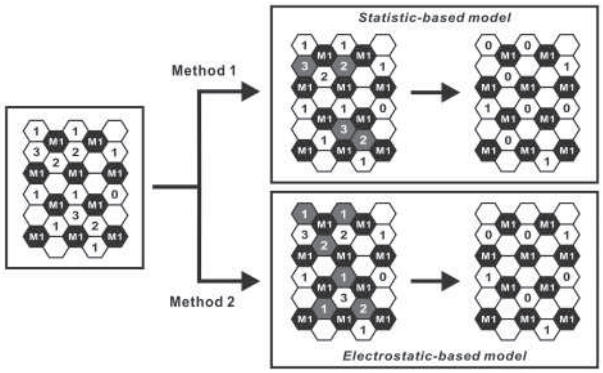

Figure 2. Schematic diagrams showing the sequences for two R^{2+}-substitution methods for R^{3+} in M_A sites to stabilize the chlorite structure. The black hexagons indicate M1 sites, and the white and gray hexagons indicate M2 sites. The hexagons labeled 1, 2, or 3 indicate the M_A sites with those numbers (1, 2, or 3) of M_A neighbors. The gray hexagons indicate those M_A sites where R^{2+}-substitutions occur as determined from each method.

TABLE 1. Assemblage data for chlorite samples

Sample	Location	Grade	Silicate phases	Opaque minerals
Assemblage data of the chlorite obtained from this work (Note: These minerals may not be in equilibrium.)				
CG/BG-6	Perry Mountain, Maine, U.S.A.	4	St+Ms+Qtz+Chl+Pl+Grt+Bt	Ilm+Gr
Ra-d86-66	Rangeley, Maine, U.S.A.	2	Grt+Chl+Qz+Pl+Ms+Bt	Ilm-Gr
Ra-d96-66	Rangeley, Maine, U.S.A.	1	Grt+Chl+Qz+Pl+Ms+Bt	Ilm-Gr-Po
Ra-o90-71	Rangeley, Maine, U.S.A.	4	Grt+Chl+Qz+Pl+Ms+Bt	Ilm-Gr-Po
Ra-d80-66	Rangeley, Maine, U.S.A.	3	Grt+Chl+Qz+Pl+Ms+Bt	Ilm-Gr-Po
Ra-d78-66	Rangeley, Maine, U.S.A.	3	Grt+Chl+Qz+Pl+Ms+Bt	Ilm-Gr-Po
Ra-o100-71	Rangeley, Maine, U.S.A.	3	Chl+Qz+Pl+Ms+Bt	Ilm-Gr-Po
Ra-a96-66	Rangeley, Maine, U.S.A.	6	Grt+St+Si+Chl+Qz+Pl+Ms+Bt	Illm-Gr-Po
Ra-c4-66	Rangeley, Maine, U.S.A.	5	Grt+St+Chl+Qz+Pl+Ms+Bt	Ilm-Gr-Po
Ra-b15-66	Rangeley, Maine, U.S.A.	5	Grt-St-Chl-And-Qz+Pl+Ms+Bt	Ilm-Gr
Ra-a49-66	Rangeley, Maine, U.S.A.	4	St+Grt+Chl+Qz+Pl+Ms+Bt	Ilm-Gr-Po
Ra-a47-66	Rangeley, Maine, U.S.A.	4	St+Grt+Chl+Qz+Pl+Ms+Bt	Ilm-Gr-Po
Ra-c1-66	Rangeley, Maine, U.S.A.	4	Qtz+Ms+St-Grt-Bt-Chl-(Ap-Tur-Mnz)	Ilm-Gr
Ra-a2-66	Rangeley, Maine, U.S.A.	5	Grt+St+Chl+Qz+Pl+Ms+Bt	Ilm-Gr-Po
Ra-a41-66	Rangeley, Maine, U.S.A.	4	St+Grt+Chl+Qz+Pl+Ms+Bt	Ilm-Gr-Po
Ra-a34-66	Rangeley, Maine, U.S.A.	5	St+Chl+Qz+Pl+Ms+Bt	Ilm-Gr-Po
Ra-c10-66	Rangeley, Maine, U.S.A.	5	St+Chl+And+Qz+Pl+Ms+Bt	Illm-Gr-Po
Ru-p18b-66	Rumford, Maine, U.S.A.	5	Sil+Bt+Qtz+Ms+Pl+Chl	Gr+Po+Rt
Ra-a86′-66	Rangeley, Maine, U.S.A.	n/a	n/a	n/a
Ru-e25-66	Rumford, Maine, U.S.A.	5	Sil+Bt+Crd+Qtz+Ms+Pl+Chl	Gr+Po+Rt
CG/BG-1	Smalls Falls, Maine, U.S.A.	1	Ms+Chl+Qtz+Pl	Gr+Ru+Po
Ru-g24-66-cor	Rumford, Maine, U.S.A.	5	St+Bt+Crd+Qtz+Ms+Pl+Chl	Gr+Po+Rt
Assemblage data of the chlorite obtained from the literature				
Likhanov 24 *	Altay-Sayan Fold Region, Russia	L/M pelite	Chl+Cld+And	
Fe-Chl †	Liskeard, Cornwall, U.K.	n/a	n/a	n/a
CA ‡	Schmiedefeld, Thüringen, Germany	n/a	n/a	n/a
CB ‡	Gobitschau, Mähren, Germany	n/a	n/a	n/a
71-62R §	Black Mountain, New Hampshire, U.S.A.	Ky-St	St+Qtz+Ms+Chl+Cld	Ilm-Mag
MVB-phRB3 #	Martello Valley, Italy	L/M phyllite	Qtz+Chl+Ms+Cld	
MVB-phRB1 #	Martello Valley, Italy	L/M phyllite	Qtz+Chl+Ms+Cld	
MVH 1181 #	Martello Valley, Italy	Hosting phyllite	Qtz+Chl+Ms+Cal+Sph	Rt
MVB-phRB2 #	Martello Valley, Italy	L/M phyllite	Qtz+Chl+Ms+Cld	
CC ‡	Oberpinzgau, Salzburg, Austria	n/a	n/a	n/a
MVB-ph1038 #	Martello Valley, Italy	L/M phyllite	Qtz+Chl+Ms+Bt+Cld	Ilm
MVB-ph1042 #	Martello Valley, Italy	L/M phyllite	Qtz+Chl+Ms	Ilm
MVB-ph1048 #	Martello Valley, Italy	L/M phyllite	Qtz+Chl+Ms+Bt+Cld	Ilm
MVB-ph1046 #	Martello Valley, Italy	L/M phyllite	Qtz+Chl+Ms	Ilm
MVB-ph1037 #	Martello Valley, Italy	L/M phyllite	Qtz+Chl+Ms	Ilm
MVB-ph1036 #	Martello Valley, Italy	L/M phyllite	Qtz+Chl+Ms	Ilm
CD ‡	Pflügelhof, Maltatal, Kärnten, Austria	n/a	n/a	n/a

* From Likhanov (1988a, 1988b).
† Pawley et al. (2002).
‡ Lougear et al. (2000).
§ Rumble (1978).
# Brigatti and Casari (1988).

in parallel with methods used for micas and described in Rancourt et al. (1996). However, we ultimately chose to fit the entire data set using an implementation of the Wivel and Mørup (1981) method as generously provided by Eddy DeGrave (University of Ghent) because fits using this software yielded more consistent parameters and had lower chi-squared values. This program, like the Rancourt method, also utilizes quadrupole-distribution functions and assumes an average correlation between isomer shift and quadrupole splitting for Fe in each site.

Widths, isomer shifts, and quadrupole splittings of all the doublets were initially allowed to vary; in final fits, the widths of one of the Fe^{3+} doublets infrequently had to be constrained. We also experimented with coupling of parameters (e.g., isomer shift) between doublets, but those fits resulted in proliferation of additional doublets that in themselves did not appear to have physical relevance. Thus, parameters reported here do not constrain coupling between doublets.

Parameters for the spectra are given in Table 3. Based on parameters from the literature (cf. Dyar et al. 2006), these samples contain Fe^{2+} and Fe^{3+} in the M sites only; precise site assignments (distributions among M1-M3 sites in chlorite) cannot be made on the basis of Mössbauer data alone.

Errors on isomer shift and quadrupole splitting of isolated peaks are usually ±0.02 mm/s, but because these spectra contain heavily overlapped peaks, the errors may be as high as ±0.05 mm/s. Errors on $Fe^{3+}/\Sigma Fe$ are ±3–5% absolute based on repeated fits to the same spectra. Errors on distributions of Fe^{2+} or Fe^{3+} among different distributions are ±5–10% absolute, again based on multiple fits to the same data; the higher uncertainty results from extensive overlap between distributions of the same valence state of Fe. Doublet areas are assumed to correspond directly to the abundances of the species present because recoil-free fractions are not known for chlorite.

X-ray diffraction experiments

Gandolfi powder-pattern simulations (Guggenheim 2005) were obtained from individual chlorite crystals using Mo radiation and a Bruker SMART APEX single-crystal diffractometer system. The use of a Gandolfi-type simulation allows for the unit-cell determination of a single grain of chlorite by a relatively large number of powder diffraction maxima. The procedure involves the averaging of nine (360°) rotation frames (i.e., "photographs") of the chlorite crystal. The nine rotation frames were obtained by systematic variations in 2θ (0, 20, and 35°) and ω (–20, 0, and 20°), such that frames were obtained at 2θ at 0° for three ω values, at 2θ at 20° for three ω values, etc. The choice of 2θ and ω allowed about a 20% overlap in each adjacent frame. Debye rings were integrated within each frame using 0.02° steps to form linear patterns that are then merged to one scale. Scaling was achieved by: (1) considering overlap for frames of equal 2θ and simple averaging, and (2) adjusting background inconsistencies for frames that differ in 2θ prior to averaging. The resulting intensity vs. 2θ scan simulates a powder pattern suitable for input to processing software; we use JADE (Materials Data, Inc.).

Procedures used a high-resolution (1024 × 1024) frame, a crystal-to-detector distance of 12 cm, a collimator with an aperture size of 0.5 mm, an exposure per frame of 1200 s, and high-resolution dark-field and flood-field corrections. The crystal-to-detector distance and the frame-center parameters were calibrated using the National Institute of Science and Technology (NIST) reference powder standard 660 for LaB_6. After this calibration, comparisons of the cell parameters of five NIST reference powder standards (674a: αAl_2O_3, TiO_2, ZnO, Cr_2O_3; 640b: Si) were made. Cell-parameter data for each standard were collected and processed in JADE by least-squares fitting. The standard errors for the cell parameters are

TABLE 2. Chemical analysis results of the Al-saturated chlorite

Sample	Si	^{IV}Al	^{VI}Al	Cr	Fe^{3+}	Fe^{2+}	Mg	Mn	Ti	Na+ Ca+K	Mg/(Mg + Fe)	$Al_T/(Al_T+$ Mg+ Fe)
Chemical composition data of the chlorite obtained from this work												
CG/BG-6	2.565	1.435	1.455	0.002	0.721	2.165	1.604	0.015	0.008	0.015	0.357	0.392
Ra-d86-66	2.658	1.342	1.449	0.005	0.247	2.495	1.713	0.027	0.005		0.385	0.385
Ra-d96-66	2.658	1.342	1.435	0.011		2.720	1.740	0.032	0.007		0.390	0.384
Ra-o90-71	2.568	1.432	1.454	0.002		2.641	1.874	0.018	0.005	0.002	0.415	0.390
Ra-d80-66	2.738	1.258	1.469	0.001	0.206	2.368	1.836	0.003	0.008		0.416	0.382
Ra-d78-66	2.564	1.436	1.481	0.004		2.611	1.881	0.008	0.006	0.005	0.419	0.394
Ra-o100-71	2.724	1.277	1.484	0.004		2.445	1.921	0.026	0.008		0.440	0.387
Ra-a96-66	2.630	1.388	1.434	0.004	0.216	2.183	2.108	0.017	0.007		0.468	0.385
Ra-c4-66	2.633	1.367	1.468	0.004		2.317	2.134	0.013	0.007		0.479	0.389
Ra-b15-66	2.673	1.377	1.622	0.005	0.304	1.869	2.041	0.010	0.006		0.484	0.416
Ra-a49-66	2.675	1.325	1.471	0.001		2.227	2.200	0.014	0.008		0.497	0.387
Ra-a47-66	2.694	1.306	1.500	0.004	0.197	1.987	2.189	0.010	0.008		0.501	0.391
Ra-c1-66	2.693	1.307	1.493	0.004	0.196	1.985	2.201	0.015	0.007		0.502	0.390
Ra-a2-66	2.657	1.343	1.488	0.003	0.147	1.956	2.306	0.014	0.007		0.523	0.391
Ra-a41-66	2.697	1.304	1.471	0.008		2.003	2.391	0.020	0.010		0.544	0.387
Ra-a34-66	2.614	1.387	1.520	0.000		1.871	2.499	0.022	0.009		0.572	0.399
Ra-c10-66	2.698	1.302	1.464	0.008		1.779	2.634	0.018	0.007		0.597	0.385
Ru-p18b-66	2.656	1.345	1.408	0.000		1.485	3.014	0.046	0.008		0.670	0.380
Ra-a86′-66	2.730	1.271	1.425	0.000		0.739	3.698	0.055	0.004		0.834	0.378
Ru-e25-66	2.687	1.314	1.421	0.000		0.517	3.975	0.027	0.004		0.885	0.378
CG/BG-1	2.686	1.315	1.445	0.001		0.495	3.936	0.050	0.005	0.001	0.888	0.384
Ru-g24-66-cor	2.700	1.301	1.433	0.000		0.256	4.214	0.026	0.004		0.943	0.379
Chemical composition data of the chlorite obtained from the literature												
Likhanov 24 *	2.510	1.490	1.520		0.496	2.604	1.330	0.020			0.300	0.405
Fe-Chl †	2.770	1.230	1.480	0.000		4.110	0.280	0.000	0.000		0.064	0.382
CA ‡	2.665	1.335	1.360	0.000		4.105	0.505	0.005	0.005		0.110	0.369
CB ‡	2.730	1.270	1.385	n/a		3.985	0.570	0.005	0.000		0.125	0.368
71-62R §	2.460	1.540	1.470			3.090	1.420				0.315	0.400
MVB-phRB3 #	2.630	1.370	1.380			3.020	1.550	0.040	0.000		0.339	0.376
MVB-phRB1 #	2.590	1.410	1.420			2.900	1.660	0.020	0.000		0.364	0.383
MVH 1181 #	2.600	1.400	1.410			2.880	1.670	0.020	0.010		0.367	0.382
MVB-phRB2 #	2.590	1.410	1.410			2.890	1.680	0.020	0.000		0.368	0.382
CC ‡	2.715	1.285	1.370	0.000		2.850	1.685	0.055	0.000		0.372	0.369
MVB-ph1038 #	2.660	1.340	1.350			2.870	1.760	0.020	0.000		0.380	0.367
MVB-ph1042 #	2.690	1.310	1.320			2.850	1.790	0.030	0.010		0.386	0.362
MVB-ph1048 #	2.640	1.360	1.360			2.830	1.790	0.010	0.010		0.387	0.371
MVB-ph1046 #	2.680	1.320	1.350			2.800	1.810	0.020	0.010		0.393	0.367
MVB-ph1037 #	2.680	1.320	1.330			2.770	1.860	0.030	0.010		0.402	0.364
MVB-ph1036 #	2.660	1.340	1.350			2.760	1.860	0.020	0.010		0.403	0.368
CD ‡	2.685	1.315	1.305	0.000		2.270	2.285	0.140	0.005		0.502	0.365

* From Likhanov (1988a, 1988b).
† Pawley et al. (2002).
‡ Lougear et al. (2000).
§ Rumble (1978).
# Brigatti and Casari (1988).

TABLE 3. Mössbauer parameters of Al-saturated chlorite

		CG/BG-6	Ra-d86-66	Ra-d80-66	Ra-a96-66	Ra-b15-66	Ra-a47-66	Ra-c1-66	Ra-a2-66	Likhanov 24
[M]Fe^{2+}	Γ	0.26	0.30	0.31	0.30	0.21	0.30	0.30	0.30	0.25
	δ	1.15	1.15	1.14	1.15	1.15	1.15	1.14	1.14	1.15
	Δ	2.68	2.67	2.63	2.67	2.61	2.66	2.64	2.67	2.51
	Area	39	91	92	92	86	92	91	93	27
[M]Fe^{2+}	Γ	0.40								0.66
	δ	1.12								1.17
	Δ	2.48								2.27
	Area	33								22
[M]Fe^{3+}	Γ	0.36		0.25		0.87		0.25		0.70
	δ	0.37		0.30		0.20		0.30		0.27
	Δ	0.94		1.08		0.73		0.92		0.99
	Area	16		2		14		2		16
[M]Fe^{3+}	Γ	0.25	0.42	0.35	0.46		0.38	0.38	0.40	
	δ	0.10	0.10	0.10	0.10		0.10	0.10	0.10	
	Δ	0.52	0.37	0.30	0.42		0.32	0.30	0.42	
	Area	8	9	6	9		9	7	7	
Ilmenite	Γ	0.47								
	δ	1.04								
	Δ	0.60								
	Area	5								
%Fe^{3+}		25	9	8	9	14	9	9	7	16
	χ^2	0.85	1.83	3.59	2.82	6.77	2.55	1.36	3.76	17.98

Notes: Γ is the linewidth of the intrinsic Lorentzian (mm/s), δ is the isomer shift (mm/s), Δ is the quadrupole splitting (mm/s), and Area is the percentage of the total area assigned to that distribution.

generally within 0.003 Å when compared to the standards as reported by NIST, although rarely errors may be as high as 0.008 Å. Cell-parameter data reported here for chlorite are those obtained from least-squares refinement in JADE. For each sample, 35 to 50 reflections with 2θ value of 2–35° (Mo radiation) were used for the cell parameters based on the monoclinic II*b* chlorite pattern (Bailey 1988). Some diffraction bands with weak or broad intensity distributions were excluded from the refinement. For several samples, multiple grains were examined to determine if there were variations of cell parameters within a single sample. In all cases, the grains examined were the same, indicating that each grain was representative of the sample.

Al-saturated chlorite models

Two types of models for Al-saturated chlorite were computer-simulated using Matlab software (MathWorks 1996). Three assumptions were made for modeling: (1) an Al-substituted tetrahedron cannot have any corner-sharing Al-substituted tetrahedral neighbors (Loewenstein 1954); (2) the model has an ideal trioctahedral chlorite structure where no vacancies exist; and (3) Al^{3+} substitution in the octahedral sheets of the 2:1 layer occurs only in smaller M2 sites and all M1 sites are occupied with R^{2+} cations. As long as assumption 2 holds, the Al^{3+} substitution for Si^{4+} in the tetrahedral sites generates the negative charge in the 2:1 layer. To balance the overall charge of the chlorite, the negative charge is compensated by Al^{3+} substitution for R^{2+} in M2 sites or in the interlayer. We initially speculated that the Al^{3+} substitution in M2 sites occurs where the sum of negative charge around the M2 sites is maximized by adjacent Al-substituted tetrahedra. One M2 site is surrounded by six coordinating O atoms comprised of four apical O atoms (two from an upper tetrahedral sheet and two from a lower tetrahedral sheet) and two O atoms from the hydroxyl groups. With assumption 1, the maximum number of the Al-substituted tetrahedral neighbors of one M2 octahedron is two, one from the tetrahedra in the upper sheet and the other from the tetrahedra in the lower sheet. The M2 site with two adjacent Al-substituted tetrahedra is hereby defined as an M_A site. Because of the charge deficiency around an M_A site, an M_A site is the most plausible M2 site where Al^{3+} substitution can occur in the octahedral sheet in the 2:1 layer.

First, we generated two independent tetrahedral sheets composed of about 180 000 tetrahedra per each sheet with cyclic boundary conditions. The tetrahedral sites were assigned randomly with either Si^{4+} or Al^{3+} following assumption 1. Because of the Al-Al avoidance rule, the probability of Al^{3+} substitution in tetrahedral sites, defined as α_n had a range of $0 \le \alpha_T \le 0.5$. After assigning the occupancy of the tetrahedral sites, we simulated a 2:1 phyllosilicate structure by orienting two opposing tetrahedral sheets at an appropriate distance such that space between the two tetrahedral sheets represents the octahedral sheet. From assumption 3, we assigned all M1 sites (on mirror planes) with R^{2+}.

One M2 site is coordinated by four apical O atoms from adjacent tetrahedra and two O atoms from hydroxyl groups. If the probability of one M2 site coordinated by *n* Al-substituted tetrahedra is defined as $p_n(\alpha_T)$, $p_n(\alpha_T)$ is expressed as:

$p_n(\alpha_T) = {}_2C_n \times ({}_2C_1\ \alpha_T)^n \times (1-{}_2C_1\alpha_T)^{2-n}$, where ${}_nC_p = n!/[p!(n-p)!]$ and $n = 0$, 1, and 2.

An M_A site was defined as an M2 site where Al^{3+} substitution can readily occur, with two Al^{3+} substitutions in neighboring tetrahedra. The probability that an M2 site is an M_A site is therefore $p_2(\alpha_T)$, which is ${}_2C_2 \times ({}_2C_1\ \alpha_T)^2 \times (1 - {}_2C_1\alpha_T)^0 = 4\ \alpha_T^2$.

Now, Al^{3+} is placed in all possible M_A sites and the remaining M2 sites are filled with R^{2+}. Because one M_A site has three edge-sharing M2 neighbors, the maximum number of the possible neighboring Al^{3+} octahedra around one M_A site is 3. An M_A site with *m* neighboring M_A sites is hereby defined as an M_{Am} site, where *m* is an integer from 0 to 3. Pauling's bond strength calculations suggest that M_{A3} and M_{A2} sites, and 5/6 of M_{A1} sites provide electrostatically less-stable configurations (see Discussion section for details). To stabilize the structure, Al^{3+} in some M_A sites must be substituted by R^{2+}. Figure 2 illustrates two methods to determine the optimal positions of R^{2+} substitutions for Al^{3+} in M_A sites. Method 1 involves the substitution of R^{2+} for Al^{3+} from more M_A-coordinated M_A sites to fewer M_A-coordinated M_A sites, e.g., in the order of $M_{A3} \rightarrow M_{A2} \rightarrow M_{A1}$ (Fig. 2). The model generated by this method is referred to as a *statistic-based model* (SB model) in that the model chlorite can contain the statistically maximum number of Al^{3+} in M_A sites by minimizing the number of R^{2+} substitutions for Al^{3+} in M_A sites. Method 2 involves charge considerations. The M_A sites have a greater charge deficiency provided from the tetrahedral sheets whereas adjacent M2 sites have a relatively smaller charge deficiency. Charge deficiency around an M_A site increases in the following order: $M_{A1}<M_{A2}<M_{A3}$. Thus, method 2 requires the substitution of R^{2+} from fewer M_A-coordinated M_A sites to more M_A-coordinated M_A sites, e.g., in the order of $M_{A1} \rightarrow M_{A2} \rightarrow M_{A3}$ (Fig. 2). The model generated by this method is referred to as an *electrostatic-based model* (EB model) in that the model allows Al^{3+} substitutions in the M_A sites, which have higher charge deficiencies than the surrounding M2 sites.

Results

Experimental results

Table 4 shows the unit-cell parameters of 39 Al-saturated chlorite samples determined by least-squares refinement. Systat software (Systat 1999) was used for the linear regression analysis of unit-cell parameters and chemical compositions. One pseudomorphic chlorite (CG/BG-6) was excluded from the regression analysis because it showed the greatest deviations in Fe^{3+}content from the other samples (25% of CG/BG-6 vs. the average of 10%). The regression equations for the unit-cell parameters were calculated as a function of Mg/(Mg + Fe) and did not consider the effect of trivalent cations. R^2 statistics were used to obtain correlation information. The analysis of variation, ANOVA test (Swan and Sandilands 1995) was performed to corroborate the confidence level of the regression. The regression equations and the statistic values are summarized in Table 5.

Mg/(Mg + Fe) shows a robust linear relationship with the *a* and *b* cell parameters (Fig. 3), with values of 0.871 and 0.889 for the R^2 statistics, respectively. The result from the ANOVA test showed that the F-statistics for the *a* and *b* cell parameters, 243.08 and 288.46, respectively, were significantly larger than 7.40 of the critical value at the 99% confidence level. The probabilities of false rejection, P_α, for both cell parameters were less than 0.01%. Moreover, as a result of the high level of confidence for the *a* and *b* cell parameters, the volume of a unit cell also showed a high confidence for a linear relationship with Mg/(Mg + Fe) (Fig. 3). However, the R^2 statistics of the regression for the volume was 0.840, which was smaller than those of the *a* and *b* cell parameters because of weak correlation of the *c* and β cell parameters with Mg/(Mg + Fe). The R^2 statistics of the *c* and β cell parameters were 0.008 and 0.073, respectively (Fig. 3). The result from the ANOVA test suggests that the *c* and β cell parameter have no significant relationship with Mg/(Mg + Fe) at the 95% confidence level (Table 5). Kepezhinskas (1965) suggested that the *c* cell parameter is linearly related to $X(^{IV}Al)$ in the tetrahedral sheets, but more careful consideration must be given for such an estimate because octahedral composition can also affect the *c* cell parameter (Rausell-Colom et al. 1991). Our results are consistent with those of Jenkins and Chernosky (1986) in which it was found that the *c* axis is sensitive to the presence/absence of co-existing phases. The data presented here, however, do not consider co-existing phases.

Modeling

We generated 215 model chlorite structures by varying the ratio of Al^{3+} substitution in the tetrahedral sites, α_T, from 0 to 0.5 with an approximately 0.002 interval. Based on the number of the edge-sharing M_A neighbors around an M_A site, the M_A sites were divided into four groups from M_{A0} to M_{A3}. Figure 4 shows the possible number of the M_A sites as a function of Mg/(Mg + Fe). The results show that the fraction of the M_A sites with a greater number of neighboring M_A sites increases as Al^{3+} substi-

TABLE 4. Unit-cell parameters of Al-saturated chlorite

Sample	Mg/(Mg + Fe)	$Al_T/(Al_T + Mg + Fe)$	Unit-cell parameters				
			a (Å)	*b* (Å)	*c* (Å)	β (°)	Volume (Å³)
X-ray diffraction data of the chlorite obtained from this work							
Likhanov 24	0.300	0.405	5.372(4)	9.313(5)	14.239(8)	97.22(5)	706.7(8)
CG/BG-6	0.357	0.392	5.381(3)	9.318(5)	14.272(10)	97.26(7)	709.8(7)
Ra-d86-66	0.385	0.385	5.374(4)	9.301(6)	14.257(8)	97.31(5)	706.7(8)
Ra-d96-66	0.390	0.384	5.361(3)	9.290(4)	14.253(9)	97.28(5)	704.1(7)
Ra-o90-71	0.415	0.390	5.362(2)	9.289(4)	14.235(5)	97.20(3)	703.4(5)
Ra-d80-66	0.416	0.382	5.365(4)	9.291(6)	14.309(15)	97.10(9)	707.7(10)
Ra-d78-66	0.419	0.394	5.373(4)	9.303(6)	14.257(18)	97.27(10)	706.9(11)
Ra-o100-71	0.440	0.387	5.365(1)	9.295(3)	14.274(6)	97.21(4)	706.1(4)
Ra-a96-66	0.468	0.385	5.361(3)	9.287(5)	14.245(12)	97.19(7)	703.6(8)
Ra-c4-66	0.479	0.389	5.360(3)	9.287(5)	14.267(10)	97.19(6)	704.6(7)
Ra-b15-66	0.484	0.416	5.356(3)	9.275(5)	14.256(11)	97.20(6)	702.6(8)
Ra-a49-66	0.497	0.387	5.362(3)	9.283(4)	14.289(10)	97.15(6)	705.7(7)
Ra-a47-66	0.501	0.391	5.364(2)	9.293(4)	14.252(10)	97.22(6)	704.8(6)
Ra-c1-66	0.502	0.390	5.360(3)	9.284(5)	14.226(13)	97.23(8)	702.3(9)
Ra-a2-66	0.523	0.391	5.354(2)	9.276(4)	14.263(9)	97.21(5)	702.8(6)
Ra-a41-66	0.545	0.387	5.356(2)	9.281(4)	14.262(8)	97.28(5)	703.2(6)
Ra-a34-66	0.572	0.399	5.352(2)	9.268(4)	14.242(8)	97.24(5)	700.8(6)
Ra-c10-66	0.597	0.385	5.347(3)	9.263(5)	14.218(9)	97.22(6)	698.6(7)
Ru-p18b-66	0.670	0.380	5.348(3)	9.260(5)	14.260(12)	97.25(7)	700.5(8)
Ra-a86′-66	0.834	0.378	5.323(2)	9.214(4)	14.274(10)	97.19(5)	694.6(6)
Ru-e25-66	0.885	0.378	5.337(2)	9.245(4)	14.238(6)	97.19(4)	697.0(5)
CG/BG-1	0.888	0.384	5.332(2)	9.236(4)	14.219(8)	97.24(5)	694.7(6)
Ru-g24-66-cor	0.943	0.379	5.318(2)	9.209(3)	14.273(7)	97.17(4)	693.5(5)
X-ray diffraction data of the chlorite obtained from the literature							
Fe-Chl *	0.064	0.382	5.396(4)	9.357(8)	14.244(6)	97.07(8)	713.7(8)
CA †	0.112	0.369	5.394(1)	9.343(1)	14.225(1)	97.35(1)	711.0(1)
CB †	0.125	0.368	5.400(1)	9.350(1)	14.234(1)	97.18(1)	713.0(1)
71-62R ‡	0.315	0.400	5.366(2)	9.298(1)	14.205(7)	97.50(4)	702.6(4)
MVB-phRB3 §	0.339	0.376	5.385(1)	9.328(1)	14.256(2)	97.48(2)	708.3(1)
MVB-phRB1 §	0.364	0.383	5.384(1)	9.324(1)	14.258(1)	97.82(1)	709.1(1)
MVH 1181 §	0.367	0.382	5.380(1)	9.321(1)	14.251(2)	97.62(1)	708.3(1)
MVB-phRB2 §	0.368	0.382	5.386(1)	9.324(2)	14.255(2)	97.76(2)	709.3(1)
CC †	0.372	0.369	5.379(1)	9.315(1)	14.248(2)	97.27(1)	708.2(2)
MVB-ph1038 §	0.380	0.368	5.383(1)	9.322(1)	14.268(1)	97.52(1)	709.8(1)
MVB-ph1042 §	0.386	0.362	5.382(1)	9.322(2)	14.271(2)	97.48(2)	709.6(2)
MVB-ph1048 §	0.387	0.371	5.378(1)	9.320(1)	14.267(1)	97.67(1)	708.7(1)
MVB-ph1046 §	0.393	0.367	5.384(1)	9.320(1)	14.272(1)	97.62(1)	709.8(1)
MVB-ph1037 §	0.402	0.364	5.376(1)	9.318(2)	14.273(3)	97.58(2)	708.7(2)
MVB-ph1036 §	0.403	0.368	5.374(1)	9.316(2)	14.264(2)	97.52(2)	708.0(2)
CD †	0.502	0.365	5.364(1)	9.291(1)	14.258(1)	97.25(1)	705.0(1)

* From Pawley et al. (2002).
† Lougear et al. (2000).
‡ Rumble (1978).
§ Brigatti and Casari (1988).

TABLE 5. Equations and statistic values from the linear regression analysis and ANOVA test

Parameters	Equations [x = Mg/(Mg + Fe)]	R^2	F-statistics *	P_α(%) †
a (Å)	$a = -0.092\,x + 5.408$	0.871	243.08	<0.01
b (Å)	$b = -0.165\,x + 9.371$	0.889	288.46	<0.01
c (Å)	$c = 0.010\,x + 14.250$	0.008	0.30	58.51
β (°)	$\beta = -0.27\,x + 97.45$	0.073	2.84	10.04
Volume (Å³)	$V = -23.38\,x + 715.84$	0.840	189.27	<0.01

* The critical values of F-statistics for 95% and 99% confidential intervals are 4.11 and 7.40, respectively.
† P_α: probability of false rejection.

tution increases. In the extreme case where Al^{3+} substitution in the tetrahedral sites reaches a maximum ($A = 0.5$), all M2 sites become M_{A3} sites (M_A sites with 3 neighboring M_A sites).

Two models (SB and EB) were developed to stabilize the chlorite structure with R^{2+} substitutions instead of Al^{3+} in M_A sites (Fig. 2). The results show that the numbers of Al^{3+} substitutions in two M2 sites vary from 0 to 1 where $A = 0.0$ and 0.5, respectively (Fig. 5). Smaller numbers of Al^{3+} can substitute in the M2 sites from the EB model than those from the SB model [e.g., 0.502(1) vs. 0.603(1) of Al^{3+} substitutions at $A = 0.4$ from EB and SB models, respectively] except for the marginal compositions, $A = 0.0$ and 0.5. The model calculations also show that most M_A sites in Al-saturated chlorite exist as isolated sites (M_{A0}) without any M_A neighbor. This result is consistent with experimental evidence that most Al cations in octahedral sites in chlorite are surrounded by six Mg octahedra based on ^{1}H and ^{27}Al MAS-NMR spectroscopy results (Welch et al. 1995).

DISCUSSION

Calculation of Al content in tetrahedral and octahedral sites of Al-saturated chlorite

Assuming that the fraction of minor elements is negligible and chlorite formed in reducing conditions where all Fe is Fe^{2+}, a generalized chemical formula of chlorite can be written as:

$$^{VI}(R^{2+}_{6-x-3y}\,Al_{x+2y}\,\square_y)\,^{IV}(Si_{4-x}\,Al_x)\,O_{10}\,(OH)_8$$

where R^{2+} = (Mg + Fe^{2+}) and □ represents a vacancy. The vari-

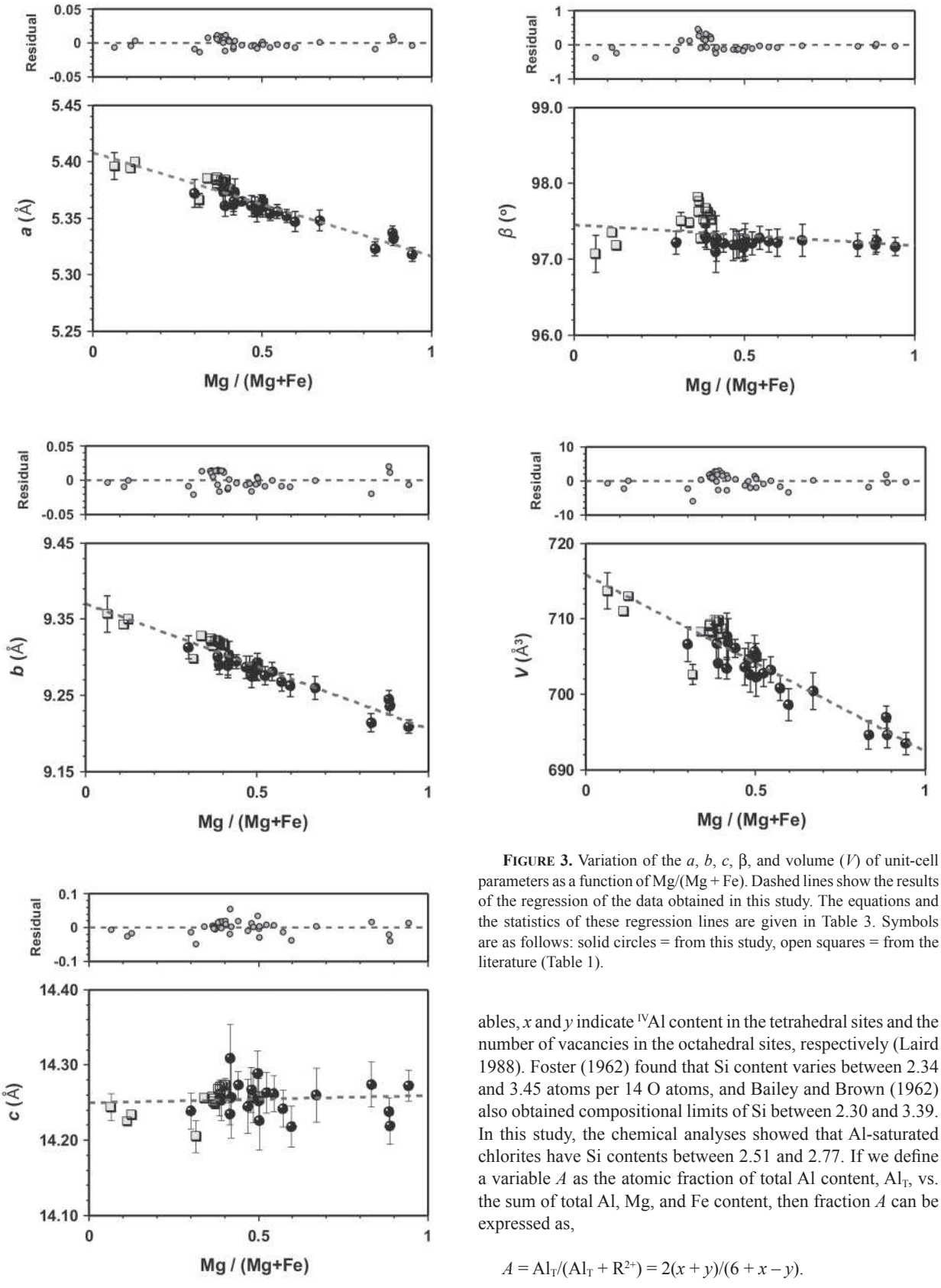

Figure 3. Variation of the *a*, *b*, *c*, β, and volume (*V*) of unit-cell parameters as a function of Mg/(Mg + Fe). Dashed lines show the results of the regression of the data obtained in this study. The equations and the statistics of these regression lines are given in Table 3. Symbols are as follows: solid circles = from this study, open squares = from the literature (Table 1).

ables, *x* and *y* indicate ^{IV}Al content in the tetrahedral sites and the number of vacancies in the octahedral sites, respectively (Laird 1988). Foster (1962) found that Si content varies between 2.34 and 3.45 atoms per 14 O atoms, and Bailey and Brown (1962) also obtained compositional limits of Si between 2.30 and 3.39. In this study, the chemical analyses showed that Al-saturated chlorites have Si contents between 2.51 and 2.77. If we define a variable *A* as the atomic fraction of total Al content, Al_T, vs. the sum of total Al, Mg, and Fe content, then fraction *A* can be expressed as,

$$A = Al_T/(Al_T + R^{2+}) = 2(x + y)/(6 + x - y).$$

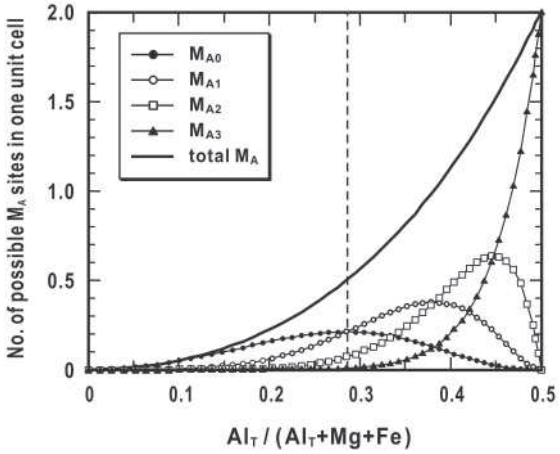

FIGURE 4. Graph showing the number of possible M_A sites in one unit cell of chlorite based on 14 oxygen equivalents. An M_A site is defined as an M2 site where Al substitution most likely occurs in the octahedral sheet in the 2:1 layer. The M_A site with *m* possible neighboring M_A sites is defined as M_{Am} where *m* can be 0, 1, 2, and 3. The dashed line indicates the composition of clinochlore (Mg end-member) and chamosite (Fe end-member) where $Al_T/(Al_T + Mg + Fe)$ is 0.286.

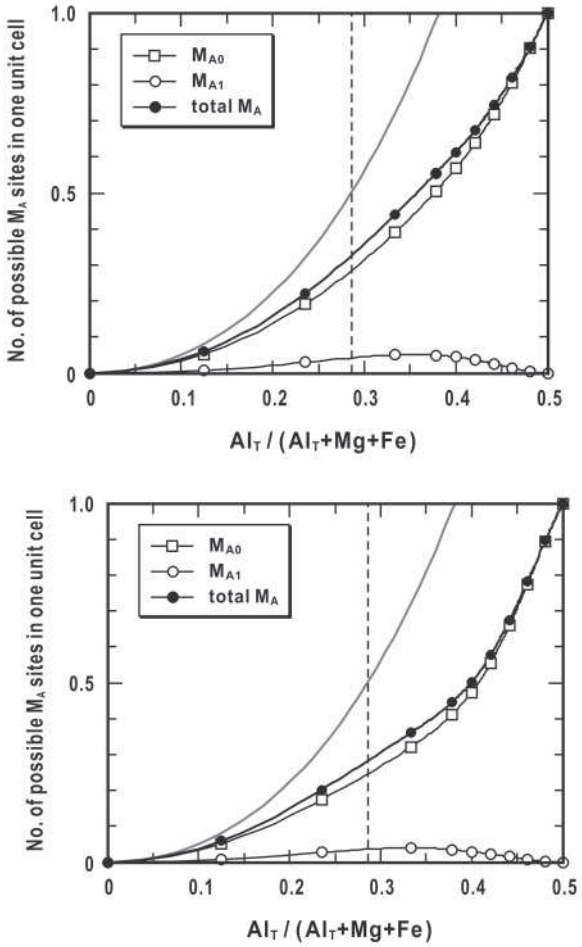

FIGURE 5. Plots showing the number of possible M_A sites in one unit cell of chlorite with 14 oxygen equivalents obtained by (upper) method 1 (a statistic-based model, SB model) and (lower) method 2 (a electrostatic-based model, EB model). The sizes of the error-bars (2σ) are smaller than the symbol sizes. The number of the total possible M_A sites given in Figure 4 (prior to applying either method) is shown with a gray line as a comparison. The compositional limit defined by clinochlore (Mg end-member) and chamosite (Fe end-member) is shown as a dashed line.

For Al-saturated chlorite with $A \approx 0.4$ [the most Al-saturated samples as shown in Laird (1988)], the value of *x* can be determined in terms of *y*:

$$0.4 = 2(x + y)/(6 + x - y) \text{ or } x = 1.5(1 - y).$$

Therefore, the variables *x* and y are dependent and in the absence of vacancies ($y = 0$), the ^{IV}Al content (x) is 1.5.

Comparison with previous regression results

According to Shirozu (1958), the *b* cell parameter is linearly correlated with Fe^{2+} content by the equation:

$$b = 9.220 \text{ Å} + 0.028 \text{ Fe}^{2+}$$

where Fe^{2+} is the number of Fe^{2+} ions in a formula unit of chlorite based on a 14 oxygen equivalent formula. Bailey (1972) also suggested a linear relationship of the *b* cell parameter with Fe^{2+} including Mn content as:

$$b = 9.210 \text{ Å} + 0.037 (\text{Fe}^{2+}, \text{Mn})$$

where Fe^{2+} and Mn are the number of Fe^{2+} and manganese in the same formula unit of chlorite as given by Shirozu. Our results cannot be compared directly to these results because chlorite data in this study have a limited Al content whereas the data of Shirozu and Bailey covered the entire range of chlorite compositions. However, these results can be compared to the earlier studies by limiting the composition of chlorite only to Al-saturated samples. The theoretical calculations (above) suggest that the Al content in the octahedral sites in Al-saturated chlorite is 1.5. Assuming that the amount of minor elements such as Mn or Ti is negligible compared to the Mg and Fe content, the sum of the Mg and Fe contents is 4.5 out of the 6 possible octahedral sites based on 14 oxygen equivalents. Thus, the equations can be transformed as a function of Mg/(Mg + Fe) and plotted on the same graph as the regression line from this study (Fig. 6). The transformed equations from Shirozu and Bailey are $b = -0.126x + 9.346$ and $b = -0.166x + 9.376$, respectively, where x = Mg/(Mg + Fe). The equation derived from Shirozu has a lower slope than the slopes from Bailey and this study and causes underestimation of the *b* unit-cell parameter for Fe-rich chlorite and overestimation for Mg-rich chlorite. In contrast, the equation derived from Bailey shows about the same slope as the equation from this study (–0.166 and –0.165, respectively), but there is a slight offset of about 0.005 Å between those two equations. However, the 0.005 Å offset has a minimal effect because it corresponds

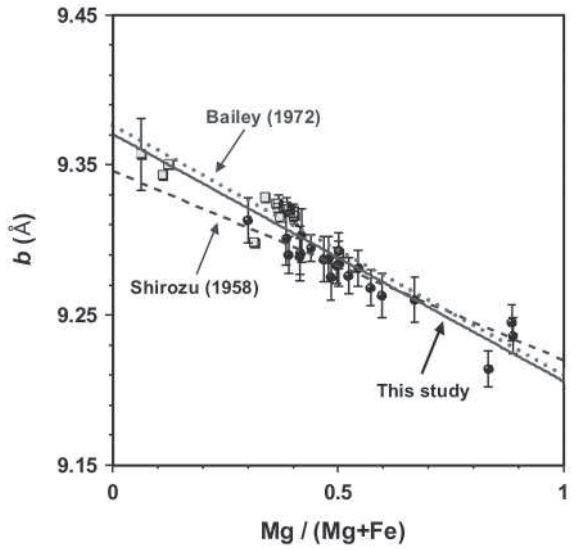

FIGURE 6. Comparison of the regression line of *b* cell parameter vs. Mg/(Mg + Fe), where all Fe is assumed as Fe^{2+}. The solid line is the regression from this study and the dotted and dashed lines are from Shirozu (1958) and Bailey (1972), respectively. Symbols are as in Figure 3.

to only about a 3% (≈0.005/0.165) difference in the value of Mg/(Mg + Fe).

Limit of Al substitution in chlorite

The Al-Al avoidance rule proposed by Loewenstein (1954), where owing to prohibitive under-bonding of the bridging O atoms, an Al-substituted tetrahedron cannot have another corner-sharing Al-substituted tetrahedral neighbor, holds true for most 2:1 layer silicates [the only exception appears to be clintonite (Takéuchi and Sadanaga 1966; Guggenheim 1984, p. 77)]. The ^{29}Si NMR spectroscopy of micas and vermiculite showed that Si-Al distributions in a tetrahedral sheet are primarily governed by Loewenstein's rule as well as the local balance of charges (Herrero et al. 1985). Electrostatic energy calculations showed that preferential long-range ordering does not exist in tetrahedral sheets, suggesting that Al ions in tetrahedral sheets may be ordered in local environments but stochastic in a long-range term (Herrero et al. 1986). The ^{29}Si MAS-NMR results for chlorite were best fitted for Al-Al avoidance in a tetrahedral sheet with a homogeneous-dispersion-charge model (Welch et al. 1995).

Substitution of Si^{4+} by Al^{3+} generates a net negative charge in the tetrahedral sheets. This net negative charge is compensated by a positive charge generated by R^{2+} substitution by R^{3+} both in octahedral sites in the interlayer and in octahedral sites in the 2:1 layer. When trivalent cations substitute for divalent cations in octahedral sites in the 2:1 layer, trivalent ions commonly occupy the smaller M2 sites rather than larger M1 sites because of the smaller ionic radii of trivalent cations (Phillips et al. 1980; Nelson and Guggenheim 1993).

Following Loewenstein's rule, the maximum number of the possible Al^{3+} substitutions in the tetrahedral sites is 2 apfu, e.g., $^{int}[Mg_2Al]^{2:1}[Mg_2Al]^{2:1}(Al_2Si_2)O_{10}(OH)_8$. In this case, half of the total tetrahedral sites are substituted by Si^{4+}, and Al^{3+}-substituted tetrahedra occur so that they alternate with Si^{4+}-substituted tetrahedra. However, the Al-saturation state in natural chlorites is obtained before reaching the maximum limit that Loewenstein's rule allows. Based on the $Al_T/(Al_T + Mg + Fe)$ fraction of 0.4 in Al-saturated chlorite (Laird 1988), the amount of Al^{3+} substituted for Si^{4+} in chlorite is 1.5 apfu, which is smaller than 2.0 apfu expected from just Al-Al avoidance-rule considerations. The difference between these two limiting values suggests that besides Loewenstein's rule, there are other factors that restrict Al^{3+} substitution in chlorite.

Consideration of the electrostatic valency rule for Al substitutions in M2 sites

Pauling's electrostatic valency rule states that in a stable structure, the total positive valence of the bonds that reach an anion from all neighboring cations is equal to the formal charge of the anion but opposite in sign. Pauling's Bond Strength (PBS) is defined as the valence charge of the cation divided by the coordination number of the cation. The PBS involves relative stability and not stability in absolute terms. Many stable structures exist for which there are significant deviations from PBS values of O atoms. These deviations may be correlated with bond lengths and quantified in terms of bond-valence sums (Brown 1978; Brown and Altermatt 1985). Although the PBS may deviate from the ideal, this is compensated by an adjustment of bond distances. Thus, at the local level, a PBS for an O atom may be low (e.g., 1.75 electrostatic valency unit, e.v.u.), but this is compensated by short bonds to that atom and a resulting increase in overall bond-valence sum to near 2.0 e.v.u. Conversely, a high PBS (e.g., 2.25 e.v.u.) is compensated by bond lengthening and a decrease in overall bond-valence sum to near 2.0 e.v.u. Nonetheless, it can be useful to consider only PBS calculations as an approximation to determine relative stability, especially if comparing very similar models with differences involving cation substitutions in a limited number of sites.

The apical O atom of a tetrahedron in the 2:1 layer is surrounded by four cations, one from the tetrahedral site and the other three from octahedral sites. The possible constitution of cations surrounding an apical O atom is a combination of either Si^{4+} or Al^{3+} from the tetrahedral site, R^{2+} from an M1 site, and either R^{2+} or Al^{3+} cations from two M2 sites. For instance, if the apical O atom of an $(SiO_4)^{4-}$ tetrahedron ($PBS_T = 4/4 = 1$) is coordinated with one M1 site having one Mg^{2+} cation and two M2 sites having two Mg^{2+} cations [e.g., Mg^{2+} in both M_A and site 1 in Fig. 7 ($PBS_{M1} = 2/6 = 1/3$, $PBS_{2M2} = 2 \times 2/6 = 2/3$)], the total PBS directed to the O atom is 2 (= 1 + 1/3 + 2/3). In this case, the structure is considered stable because the apical O atom is saturated with respect to charge. However, when both neighboring M2 sites are substituted by Al^{3+} (e.g., Al^{3+} in both M_A and site 1 in Fig. 7) the calculated PBS of the apical O atom of an $(SiO_4)^{4-}$ tetrahedron is 2.33, which deviates from the formal charge of the O ion. A similar situation occurs for the O atoms of the hydroxyl groups when the O atoms are shared by two Al^{3+}-substituted M2 sites (e.g., Al^{3+} in both M_A and site 3 in Fig. 7). Table 6 summarizes the PBS values of the O atoms surrounding an M_A site with possible site occupancies in the neighboring M2 sites. Based on Pauling's electrostatic valency rule, the discrepancy between the PBS and the formal charge of

TABLE 6. PBS of four apical oxygen atoms of tetrahedra and two oxygen atoms of hydroxyl groups surrounding an M_A site occupied by Al^{3+}

M_A	Site 1	Site 2	Site 3	Where the tetrahedron of a given apical oxygen (O1…O4) contains		PBS of the apical oxygen (O1…O4)	
				O1	O2	O1	O2
Al^{3+}	Al^{3+}			Si^{4+}	Si^{4+}	2.33	2.33
				Si^{4+}	Al^{3+}	2.33	2.08
				Al^{3+}	Si^{4+}	2.08	2.33
				Al^{3+}	Al^{3+}	2.08	2.08
Al^{3+}	R^{2+}			Si^{4+}	Si^{4+}	2.17	2.17
				Si^{4+}	Al^{3+}	2.17	1.92
				Al^{3+}	Si^{4+}	1.92	2.17
				Al^{3+}	Al^{3+}	1.92	1.92
				O3	O4	O3	O4
Al^{3+}		Al^{3+}		Si^{4+}	Si^{4+}	2.33	2.33
				Si^{4+}	Al^{3+}	2.33	2.08
				Al^{3+}	Si^{4+}	2.08	2.33
				Al^{3+}	Al^{3+}	2.08	2.08
Al^{3+}		R^{2+}		Si^{4+}	Si^{4+}	2.17	2.17
				Si^{4+}	Al^{3+}	2.17	1.92
				Al^{3+}	Si^{4+}	1.92	2.17
				Al^{3+}	Al^{3+}	1.92	1.92
				PBS of the oxygen atoms of hydroxyl groups			
				O5		O6	
Al^{3+}			Al^{3+}	2.33		2.33	
Al^{3+}			R^{2+}	2.17		2.17	

Note: The notations of the sites and oxygen atoms are given in Figure 7.

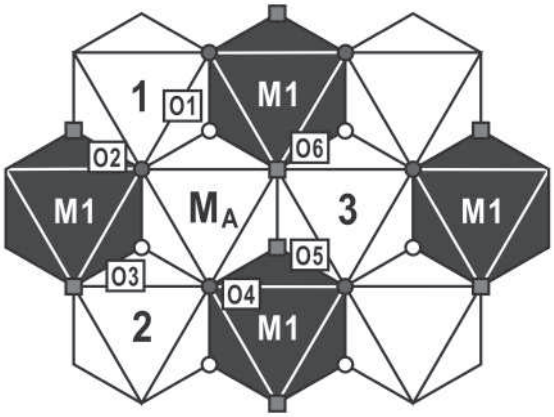

FIGURE 7. Schematic diagram showing three M2 neighbors around one M_A site. The apical O atoms of the tetrahedra in the upper sheet and in the lower sheet are shown as solid and open circles, respectively. The O atoms of the hydroxyl groups are shown as solid squares. Sites 1 and 2 are M2 sites sharing two apical O atoms of the tetrahedra with the M_A site. Site 3 shares two O atoms of the hydroxyl groups with the M_A site. The O atoms surrounding the M_A site are labeled from O1 to O6. The calculation of the Pauling's bond strength (PBS) of the O atoms surrounding the M_A site is given in Table 6 with regard to the cations in the M2 neighbors.

the O ion will make the structure less stable relative to a structure where all charges balance between neighbors.

The models (SB and EB) based on the electrostatic valency rule suggest one possible reason why Al-saturated chlorite reaches its Al maximum at lower Al contents than 0.5. In the models, we compared a basic chlorite structure with deviations only in the pattern of substitution of Al in tetrahedral and octahedral sites, but did not consider possible effects of bond distances. The model calculations show the limit of Al^{3+} substitution for R^{2+} in the octahedral sites in the 2:1 layer. Whereas Al^{3+} substitution for R^{2+} at M2 sites compensates a net negative charge on apical O atoms generated by Al^{3+} substitution for Si^{4+} in neighboring tetrahedra, these substitutions can also generate excess positive charge on O atoms around the octahedral sites, particularly when M_A sites share O atoms with other neighboring M_A sites. The modeling shows that most M_A sites in Al-saturated chlorite exist as isolated sites (M_{A0}) without any M_A neighbor. This isolation occurs because two adjacent Al-substituted M_A sites can be stabilized only when they share two Al-substituted tetrahedra with their M_A neighbor (Table 6). The probability of existence of two successive Al-substituted M_A sites is 1/6 out of the total possible two adjacent M_A site configurations, because: (1) only site 1 and 2 in Figure 7 share apical O atoms of adjacent tetrahedra with an M_A site (probability of 2/3), and (2) the probability that two adjacent M_A sites share two apical O atoms from two Al-substituted tetrahedra is $(1/2)^2$.

Layer-charge considerations

The assumption of an ideal trioctahedral chlorite excludes the effect of octahedral vacancies. Therefore, all negative charge is generated by Al^{3+} substitution for Si^{4+} in the tetrahedral sites, and this charge is compensated by the positive charge generated by Al^{3+} substitution in the octahedral sheet in the 2:1 layer and in the octahedral sheet in the interlayer. The amount of negative charge originating from the tetrahedral sheets can be expressed as $-4\alpha_T$ in one unit cell of chlorite with 14 oxygen equivalents. If the positive charge in the octahedral sites in the 2:1 layer and the positive charge in the interlayer are defined as $C^0_{2:1}$ and C_{Int}, respectively, the overall charge of chlorite is $C_{\text{Int}} - (4\alpha_T - C^0_{2:1})$. To balance the overall charge of the chlorite structure, the interlayer charge, C_{Int} must be equal to $(4\alpha_T - C^0_{2:1})$.

Figure 8 shows that the layer-charge of Al-saturated chlorite with $A = 0.4$ is approximately 0.89 for the SB model. Rule and Bailey (1987) suggested that when chlorite has highly Al-substituted tetrahedral sheets, the layer charge of the chlorite approaches 1.0. The SB model was generated to contain the (statistically) maximum number of Al^{3+} in M_A sites. The discrepancy of the layer charges between the calculated value from the SB model and values from natural Al-saturated chlorites implies that the substitution of Al^{3+} in M2 sites is not simply related to maximizing the number of Al^{3+} substitutions in M2 sites. In contrast, the EB model generated by method 2 is based on charge balance such that Al^{3+} substitution in the octahedral sites in the 2:1 layer occurs in energetically favorable M_A sites. The EB model calculation showed that the layer charge of Al-saturated chlorite with $A = 0.4$ is approximately 1.00. This results in the same value for the layer charge as suggested by Rule and Bailey (1987). The implication is that the Al^{3+} substitution in the octahedral sites in the 2:1 layer in Al-saturated chlorite occurs selectively in energetically favorable M_A sites. These energetically favorable M_A sites occur where the negative charge from neighboring Al-tetrahedra is more generally distributed throughout the tetrahedral sheets

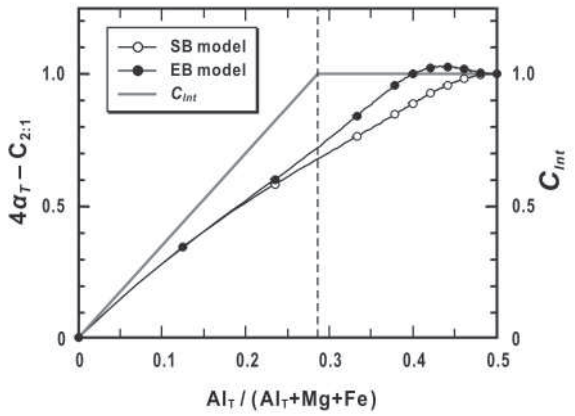

FIGURE 8. Graph showing layer-charge variations in the 2:1 layer and in the interlayer as a function of atomic $Al_T/(Al_T + Mg + Fe)$ in chlorite. $4\alpha_T$ and $C^0_{2:1}$ indicate the negative charge from the tetrahedral sheets and the positive charge from the octahedral sheet in the 2:1 layer, respectively, and C_{Int} indicates the positive charge from the interlayer of chlorite. The sizes of the error-bars (2σ) are smaller than the symbol sizes. The dashed line indicates the composition of clinochlore (Mg end-member) and chamosite (Fe end-member). The interlayer charge of chlorite with a Al^{3+} content below the clinochlore-chamosite composition line is estimated to be the same as the amount of Al^{3+} substitution for Si^{4+} in the tetrahedral sites.

compared to their neighboring M2 sites with less negative-charge distributions from Al-tetrahedra.

Note that when *A* is 0.4, the interlayer charge to compensate the negative charge from the 2:1 layer is 1.0. Ideally, the interlayer can have one charge (e.v.u.) per unit cell when R^{2+} and Al^{3+} cations are alternatively positioned in the M4 sites. When *A* is between 0.4 and 0.5, the EB model suggests that the 2:1 layer of the Al-saturated chlorite has a layer charge of ≤ -1. To balance the charge, the interlayer requires more Al^{3+} substitution for R^{2+} in M4 sites than the idealized structure. Such a configuration inevitably requires some Al-substituted M4 sites sharing the hydroxyl groups with adjacent Al-substituted M4 sites. If the same PBS constraint is applied, the structure will cause destabilization of the O atoms of the hydroxyl groups because they are coordinated by two adjacent Al-substituted M4 sites in the interlayer (PBS = 2.33). Therefore, the limitation ($A = 0.4$) in Al content of natural chlorites is probably related to the electrostatic restriction of Al substitutions in the octahedral sites both in the 2:1 layer and in the interlayer. Moreover, the reason why idealized chlorite $^{int}(Mg_2Al)^{2:1}(Mg_2Al)^{2:1}(Si_2Al_2)O_{10}(OH)_8$ is rare may be related to the O destabilization, which prohibits Al substitution in the interlayer of more than 1 apfu as a kinematic barrier to more Al^{3+} substituting in the chlorite structure.

In summary, the electrostatic models of Al-saturated chlorite suggest that there are restrictions on Al^{3+} substitution in octahedral sites as determined from Pauling's rules. Thus, Al saturation is reached before the idealized chemical composition of half of the tetrahedral sites being occupied with Al^{3+}. The results from model calculations are also applicable to the trioctahedral micas that have reached equilibrium. These micas also show an Al-saturation limit before half of the tetrahedral sites are substituted with Al^{3+} (Crowley and Roy 1964; Hewitt and Wones 1975).

ACKNOWLEDGMENTS

We gratefully acknowledge the microprobe analyses performed by Marty Yates, University of Maine, Orono, Maine, Mössbauer fits by Elizabeth Sklute and Yarrow Rothstein, and the assistance of Edward S. Grew and John T. Cheney in retrieving information from Guidotti's records. We thank J. Post, Smithsonian Institution, Washington, and M. Welch, Natural History Museum, London, for perceptive reviews. We further acknowledge the support of the National Science Foundation for funding under grant EAR-0308588 and EAR-0308546. Although C.V. Guidotti is a co-author, we dedicate this paper to his memory. Unfortunately, he passed away midway through the project, and his expertise was sorely missed as we proceeded. We will miss him as both colleague and friend.

REFERENCES CITED

Bailey, S.W. (1972) Determination of chlorite composition by X-ray spacings and intensities. Clays and Clay Minerals, 20, 381–388.

——— (1988) Chlorites: Structure and crystal chemistry. In S.W. Bailey, Ed., Hydrous Phyllosilicates, 19, p. 347–403. Reviews in Mineralogy, Mineralogical Society of America, Chantilly, Virginia.

Bailey, S.W. and Brown, B.E. (1962) Chlorite structural variations. Special Paper, Geological Society of America, pp.130.

Baker, J. and Holland, T.J.B. (1996) Experimental reversals of chlorite compositions in divariant $MgO + Al_2O_3 + SiO_2 + H_2O$ assemblages. American Mineralogist, 81, 676–684.

Brigatti, M.F. and Casari, L. (1988) Chlorites from cobalt pyrite horizons, Upper Martelle Valley (Alto Adige, northern Italy). Neues Jahrbuch für Mineralogie Monatshefte, 1988, 547–558.

Brown, I.D. (1978) Bond valences. A simple structural model for inorganic chemistry. Chemical Society Reviews, 7, 359–376.

Brown, I.D. and Altermatt, D. (1985) Bond-valence parameters obtained from a systematic analysis of the inorganic crystal structure database. Acta Crystallographica, Section B: Structural Science, 41, 244–247.

Crowley, M.S. and Roy, R. (1964) Crystalline solubility in the muscovite and phlogopite groups. American Mineralogist, 49, 348–362.

Dyar, M.D., Guidotti, C.V., Harper, G.D., McKibben, M.A., and Saccocia, P.J. (1992) Controls on ferric iron in chlorite. Geological Society of America Abstracts with Programs, 1992 Annual Meeting, 338 p.

Dyar, M.D., Agresti, D.G., Schaefer, M., Grant, C.A., and Sklute, E.C. (2006) Mössbauer spectroscopy of earth and planetary materials. Annual Reviews of Earth and Planetary Science, 34, 83–125.

Eggleton, R.A. and Bailey, S.W. (1967) Structural aspects of dioctahedral chlorite. American Mineralogist, 52, 673–689.

Foster, M.D. (1962) Interpretation of the composition and a classification of the chlorites. U.S. Geological Survey Professional Paper Report: P414-A, 1–15.

Guggenheim, S. (1984) The brittle micas. In S.W. Bailey, Ed., Micas, 13, p. 61–104. Reviews in Mineralogy, Mineralogical Society of America, Chantilly, Virginia.

——— (2005) Simulations of Debye-Scherrer and Gandolfi patterns using a Bruker SMART/APEX Diffractometer System. Bruker AXS Application Note 373, 8p. Madison, Wisconsin; see also American Crystallographic Annual Meeting, Chicago, Illinois, July 2004, abstract, 182 p.

Guidotti, C.V. (1974) Transition from staurolite to sillimanite zone, Rangeley Quadrangle, Maine. Geological Society of America Bulletin, 85, 475–490.

Guidotti, C.V., Teichmann, F., and Henry, D.J. (1991) Chlorite-bearing polymetamorphic metapelites in the Rangely area, Maine: evidence for equilibrium assemblages. American Mineralogist, 76, 867–879.

Herrero, C.P., Sanz, J., and Serratosa, J.M. (1985) Si, Al distribution in micas: analysis by high-resolution ^{29}Si NMR spectroscopy. Journal of Physics C: Solid State Physics, 18, 13–22.

——— (1986) The electrostatic energy of micas as a function of Si, Al tetrahedral ordering. Journal of Physics C: Solid State Physics, 19, 4169–4181.

Hewitt, D.A. and Wones, D.R. (1975) Physical properties of some synthetic Fe-Mg-Al trioctahedral biotites. American Mineralogist, 60, 854–862.

Jenkins, D.M. and Chernosky, J.V., Jr. (1986) Phase equilibria and crystallochemical properties of Mg-chlorite. American Mineralogist, 71, 924–936.

Kepezhinskas, K.B. (1965) Composition of chlorites as determined from their physical properties. Doklady Akad Nauk. S.S.S.R., Earth Science Section, 164, 126–129.

Laird, J. (1988) Chlorites: metamorphic petrology. In S.W. Bailey, Ed., Hydrous Phyllosilicates, 19, p. 405–453. Reviews in Mineralogy, Mineralogical Society of America, Chantilly, Virginia.

Likhanov, I.I. (1988a) Chloritoid, staurolite and gedrite of the high-alumina hornfelses of the Karatash pluton. International Geology Review, 30, 868–877.

——— (1988b) Evolution of chemical composition of metapelite minerals during low-grade contact metamorphism. International Geology Review, 30, 878–887.

Loewenstein, W. (1954) The distribution of aluminum in the tetrahedra of silicates and aluminates. American Mineralogist, 39, 92–96.

Long, G.J., Cranshaw, T.E., and Longworth, G. (1983) The ideal Mössbauer effect

absorber thicknesses. Mössbauer Effect Reference Data Journal, 6, 42–49.
Lougear, A., Grodzicki, M., Bertoldi, C., Trautwein, A.X., Steiner, K., and Amthauer, G. (2000) Mössbauer and molecular orbital study of chlorites. Physics and Chemistry of Minerals, 27, 258–269.
MathWorks (1996) Matlab: The language of technical computing version 5. 86 p. MathWorks, Inc., Natick, Massachusetts.
Nelson, D.O. and Guggenheim, S. (1993) Inferred limitations to the oxidation of Fe in chlorite: a high temperature single-crystal X-ray study. American Mineralogist, 78, 1197–1207.
Pawley, A.R., Clark, S.M., and Chinnery, N.J. (2002) Equation of state measurements of chlorite, pyrophyllite, and talc. American Mineralogist, 87, 1172–1182.
Phillips, T.L., Loveless, J.K., and Bailey, S.W. (1980) Cr^{3+} coordination in chlorites: a structural study of ten chromium chlorites. American Mineralogist, 65, 112–122.
Rancourt, D.G. and Ping, J.Y. (1991) Voigt-based methods for arbitrary-shape static hyperfine parameter distributions in Mössbauer spectroscopy. Nuclear Instruments & Methods in Physics Research Section B - Beam Interactions with Materials and Atoms, 58, 85–97.
Rancourt, D.G., Ping, J.Y., Boukili, B., and Robert, J.-L. (1996) Octahedral site Fe^{2+} quadrupole splitting distributions from Mössbauer spectroscopy along the (OH,F)-annite join. Physics and Chemistry of Minerals, 23, 63–71.
Rausell-Colom, J.A., Wiewióra, A., and Matesanz, E. (1991) Relationship between composition and d_{001} for chlorite. American Mineralogist, 76, 1373–1379.
Roots, M. (1994) Molar volumes on the clinochlore-amesite binary: some new data. European Journal of Mineralogy, 6, 279–283.
Rule, A.C. and Bailey, S.W. (1987) Refinement of the crystal structure of a monoclinic ferroan clinochlore. Clay and Clay Minerals, 35, 129–138.
Rumble, D. (1971) Fe-Ti oxide minerals and the behavior of oxygen during regional metamorphism. Year Book, Carnegie Institution of Washington, 70, 157–165.
——— (1978) Mineralogy, petrology, and oxygen isotope geochemistry of the Clough Formation, Black Mountain, Western New Hampshire. Journal of Petrology, 19, 317–340.
Rumble, D., Ferry, J.M., Spear, F.S., and Chamberlain, C.P. (1993) Petrologic and isotopic studies in metamorphic rocks of Eastern Vermont and Western New Hampshire. In J.T. Cheney and J.B. Brady, Eds., Guidebook, Field Trip for the Northeastern U.S., D-1-D-33. Geological Society of America, Washington, D.C.
Shirozu, H. (1958) X-ray powder patterns and cell dimensions of some chlorites in Japan, with a note on their interference colors. Journal of Mineralogy (Japan), 2, 209–223.
Shirozu, H. and Higashi, S. (1976) Structural investigations of sudoite and regularly interstratified sericite/sudoite. Mineralogical Journal (of Japan), 8, 158–170.
Swan, A.R.H. and Sandilands, M. (1995) Introduction to Geological Data Analysis. 446 p. Blackwell Science Inc., Malden, Massachusetts.
Systat (1999) Systat 9: Getting Started, 188 p. Systat Software, Inc., Chicago, Illinois.
Takéuchi, Y. and Sadanaga, R. (1966) Structural studies of brittle micas. (I) the structure of xanthophyllite refined. Mineralogical Journal, 4, 424–437.
Welch, M.D., Barras, J., and Klinowski, J. (1995) A multinuclear NMR study of clinochlore. American Mineralogist, 80, 441–447.
Wivel, C. and Mørup, S. (1981) Improved computational procedure for evaluation of overlapping hyperfine parameter distributions in Mössbauer spectra. Journal of Physics E: Scientific Instruments, 14, 605–610.

Manuscript received May 11, 2006
Manuscript accepted January 11, 2007
Manuscript handled by Warren Huff